# Supporting Information

**Molecular superoxide radical photogeneration in cancer cells by dipyridophenazine iridium(III) complexes**

Vojtech Novohradsky,[a,+] Gloria Vigueras,[b,+] Jitka Pracharova,[c] Natalia Cutillas,[b] Christoph Janiak,[d] Hana Kostrhunova,[a] Viktor Brabec,[a] José Ruiz,*[,b] and Jana Kasparkova*[,a]

[a]Institute of Biophysics, Czech Academy of Sciences, Kralovopolska 135, 612 65 Brno, Czech Republic, Email: jana@ibp.cz.
[b]Departamento de Química Inorgánica, Universidad de Murcia and Institute for Bio-Health Research of Murcia (IMIB-Arrixaca), E-30071 Murcia, Spain Tel: + 34 868887455,  Email: jruiz@um.es.
[c]Department of Biophysics, Centre of the Region Hana for Biotechnological and Agricultural Research, Palacky University, Slechtitelu 27, 783 71 Olomouc (Czech Republic).
[d]Institut für Anorganische Chemie und Strukturchemie, Heinrich-Heine-Universität Düsseldorf, Universitätsstr 1, 40225 Düsseldorf, Germany.
[+] These authors contributed equally to this work.

# Table of Contents

**Synthesis of HC^N proligands.**

*Preparation of 2-(naphthalen-2-yl)-1H-benzo[d]imidazole (HL$^{2a}$):*



**Scheme S1**.

Proligand **HL$^{2a}$** was synthesized using an adaptation method of reference.[1] 2-Naphthaldehyde (7.77 mmol) and o-phenylenediamine (7.4 mmol) were dissolved in 2 ml of DMF. The mixture was stirred at 80ºC for 5 days. Then, the reaction mixture was suspended in 30 mL of dichloromethane and was extracted with water (5 x 60 mL). The organic layer was dried over Mg$_2$SO$_4$, filtered and the solvent was removed under reduced pressure. The residue was stirred with diethyl ether for 3 h, and the solid was filtered. Brown solid. Isolated yield: 40%. Reported.[1]

*Preparation of 2-(thiophen-2-yl)-1H-benzo[d]imidazole (HL$^{3a}$):*
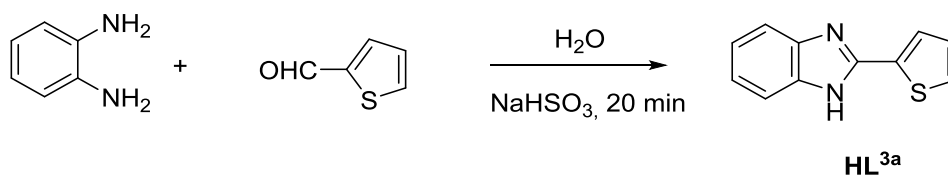


**Scheme S2**.

Proligand **HL$^{3a}$** was synthesized with a slight modification of method of literature.[2] Thiophene-2-carbaldehyde (1.0 mmol) and NaHSO$_3$ (11.0 eq, 1.14 g) was dissolved in H$_2$O (4.0 mL). When the mixture reached refluxing temperature, o-phenylenediamine (1.0 mmol) was added. The resulting mixture was stirred for 20 min. Then, the solid was filtered, washed with water (2 x 4 mL), and air-dried.
Pale yellow solid. Isolated yield: 78%. Reported.[3]

*Preparation of proligands **HL$^{1b-3b}$**:*
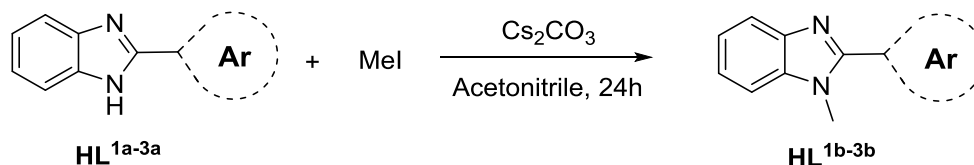


**Scheme S3**.

The N-methylation was performed with a modification of method of literature.[4]

A suspension of **HL**[1a-3a] (1 mmol), cesium carbonate (1.5 mmol) and the methyl iodide (1.8 mmol) in acetonitrile (1 mL/ 0.1 mmol benzimidazole) was stirred at room temperature for 24 h under nitrogen atmosphere. The progress of reaction was monitored by TLC. After completion of the reaction, the mixture was concentrated in vacuo. The residue was suspended in a mixture of $CH_2Cl_2$ and sat. $NaHCO_3$ (vol % 50:50, 10 mL/0.1 mmol **HL**[1a-3a]). The aqueous layer was extracted with $CH_2Cl_2$ (2 x 10 mL/0.1 mmol **HL**[1a-3a]). The combined organic layers were dried over $Mg_2SO_4$, filtered and the solvent was removed under reduced pressure. The crude product was purified by column chromatography on silica gel using ethyl acetate/hexane (2:3) as eluent.

1-methyl-2-phenyl-1H-benzo[d]imidazole (**HL**[1b]). Brown solid. Isolated yield: 74%. Reported.[5]

1-methyl-2-(naphthalen-2-yl)-1H-benzo[d]imidazole (**HL**[2b]). Brown solid. Isolated yield: 51%. Reported.[6]

1-methyl-2-(thiophen-2-yl)-1H-benzo[d]imidazole (**HL**[3b]). Brown solid. Isolated yield: 70%. Reported.[7]

*Preparation of proligands HL*[1c-3c]:
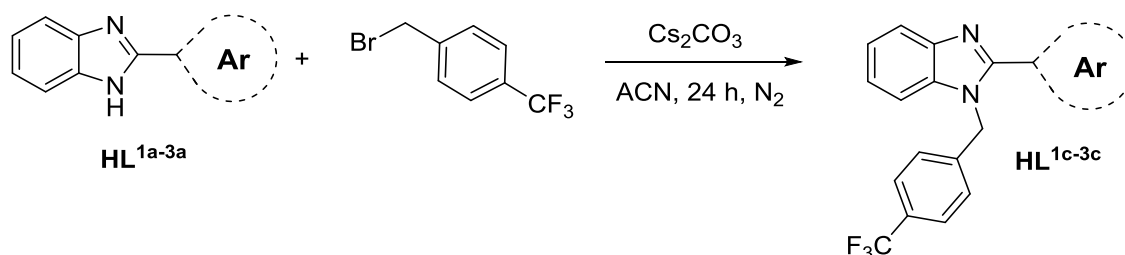


**Scheme S4**.

The N-benzylation was performed as previously reported.[4] A suspension of **HL**[1a-3a] (1 mmol), cesium carbonate (1.5 mmol) and the 1-(bromomethyl)-4-(trifluoromethyl)benzene (1.05 mmol) in acetonitrile (1 mL/ 0.1 mmol benzimidazole) was stirred at room temperature for 24 h under nitrogen atmosphere. The progress of reaction was monitored by TLC. After completion of the reaction, the mixture was concentrated in vacuo. The residue was suspended in a mixture of $CH_2Cl_2$ and sat. $NaHCO_3$ (vol % 50:50, 10 mL/0.1 mmol **HL**[1a-3a]). The aqueous layer was extracted with $CH_2Cl_2$ (2 x 10 mL/0.1 mmol **HL**[1a-3a]). The combined organic layers were dried over $Mg_2SO_4$, filtered and the solvent was removed under reduced pressure.

2-phenyl-1-[4-(trifluoromethyl)benzyl]-1H-benzo[d]imidazole (**HL**[1c]). White solid. Isolated yield: 92%. Reported.[4]

2-(naphthalen-2-yl)-1-(4-(trifluoromethyl)benzyl)-1H-benzo[d]imidazole (**HL**[2c]). Pale brown solid. Isolated yield: 80%. ^{1}H-NMR (400 MHz, CDCl3): δ 8.14 (s, 1H), 7.95 (d, J= 3.2 Hz,1H), 7.93 (d, J= 3.6 Hz, 1H), 7.89 (d, J= 7.6 Hz, 1H), 7.78 (m, 2H), 7.62 (d, J= 8.4 Hz, 2H), 7.55 (m, 3H), 7.37 (m, 1H), 7.24 (m, 4H), 5.57 (s, 2H). m/z = 403.1426 [M+H]⁺.

4

2-(thiophen-2-yl)-1-(4-(trifluoromethyl)benzyl)-1H-benzo[d]imidazole (**HL³c**). White solid. Isolated yield: 87%. ¹H-NMR (300 MHz, CDCl₃): 7.86 (dd, J= 0.6, 8.0 Hz, 1H), 7.59 (d, J= 8.2 Hz, 2H), 7.49 (m, 1H), 7.26 (m, 6H), 7.08 (m, 1H), 5.64 (s, 2H). m/z = 359.081 [M+H]⁺.

**Synthesis of precursor iridium chloro-bridged dimers [Ir(μ-Cl)(C^N)₂]₂ I–IX**
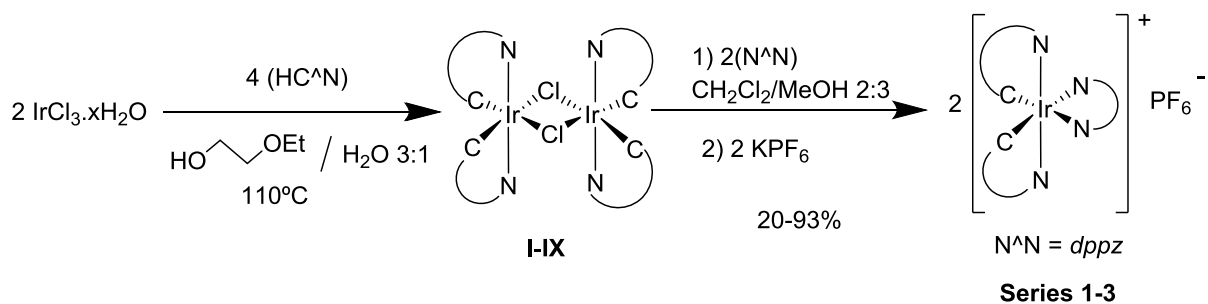


**Scheme S5**.

**Dimers I–XI** were prepared by variation of the standard literature procedures for other bridged-chloride dimers. [4, 8-10] The corresponding **HC^N** proligand (2.2 mmol) and IrCl₃·3H₂O (1 mmol) was dissolved in 2-ethoxyethanol/deionized H₂O (3:1) in a round bottom flask. The reaction was stirred at 110 °C for 24 h under nitrogen atmosphere. The mixture was cooled down to room temperature and the resultant solid was collected by filtration. The solid was washed with water and ethanol. The products were used in subsequent reaction without further purification.
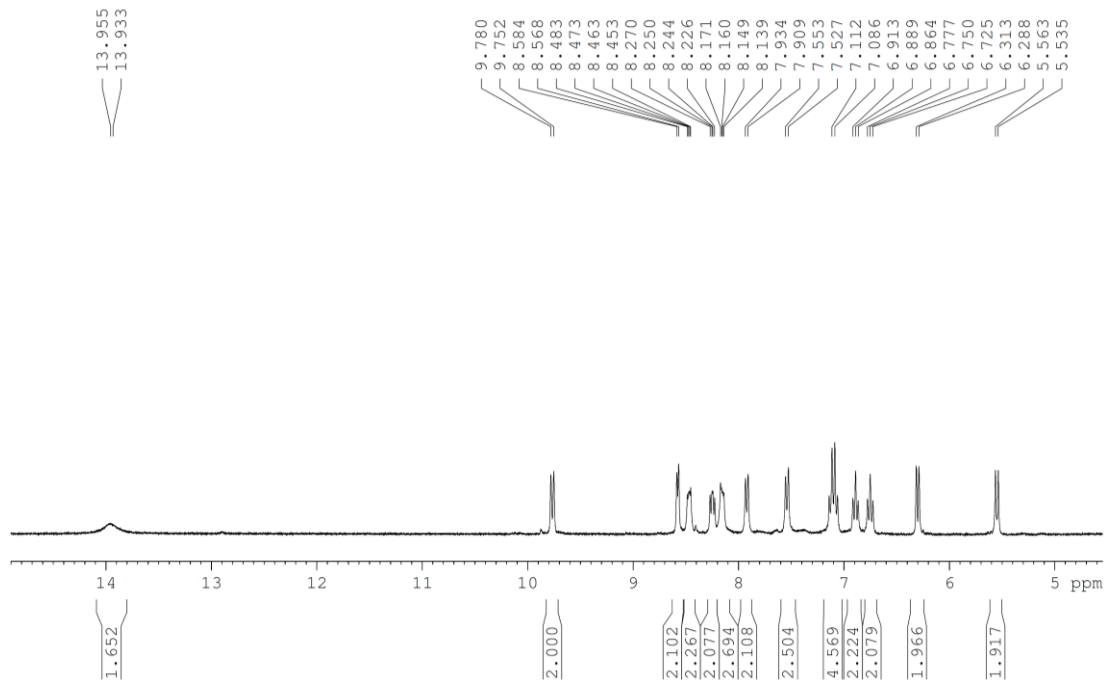
**Figure S1**. $^1$H NMR in DMSO-d$_6$ for **1a**.
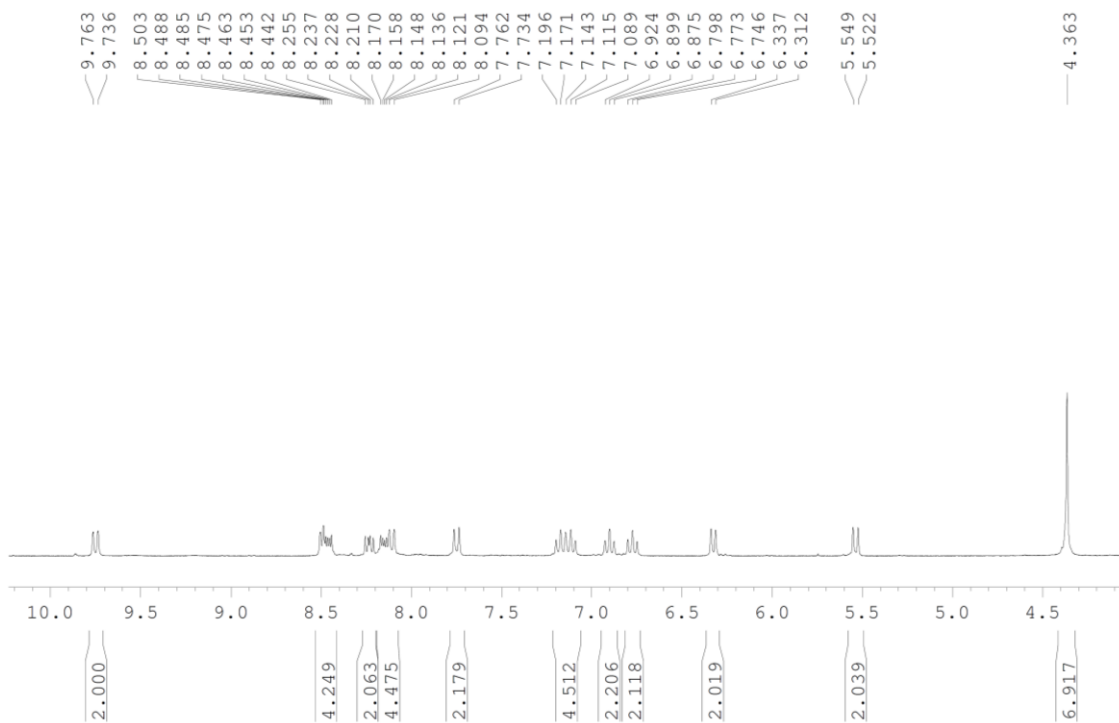


**Figure S2**. $^1$H NMR in DMSO-d$_6$ for **1b**.
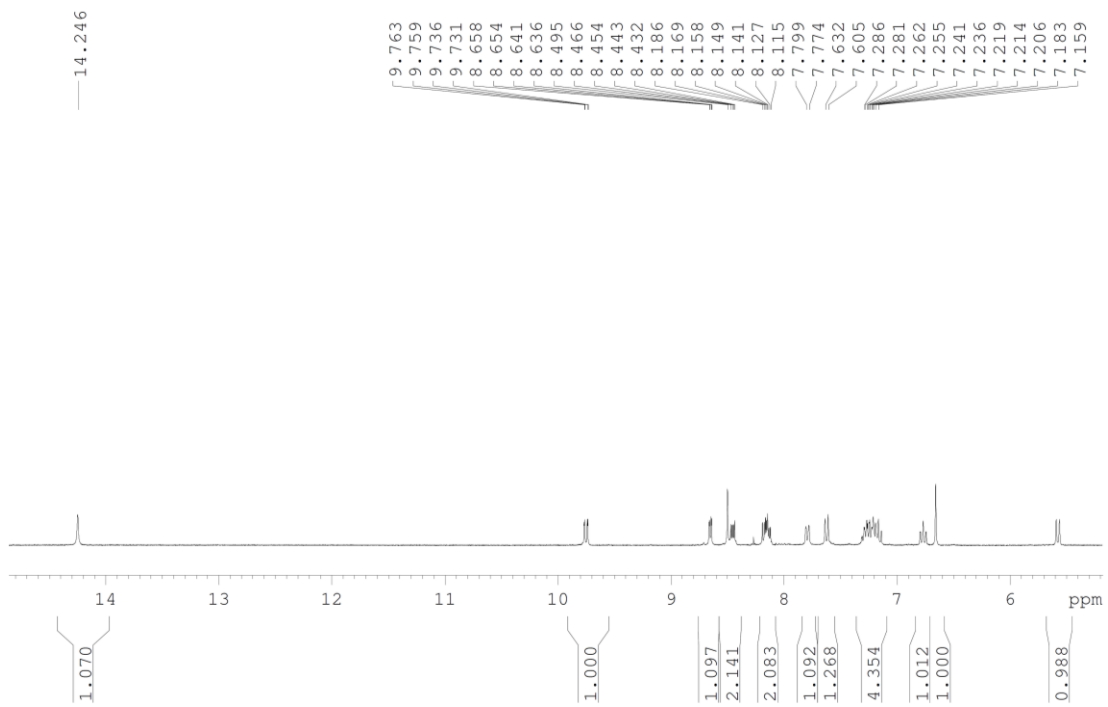
**Figure S3**. $^1$H NMR in DMSO-$d_6$ for **2a**.
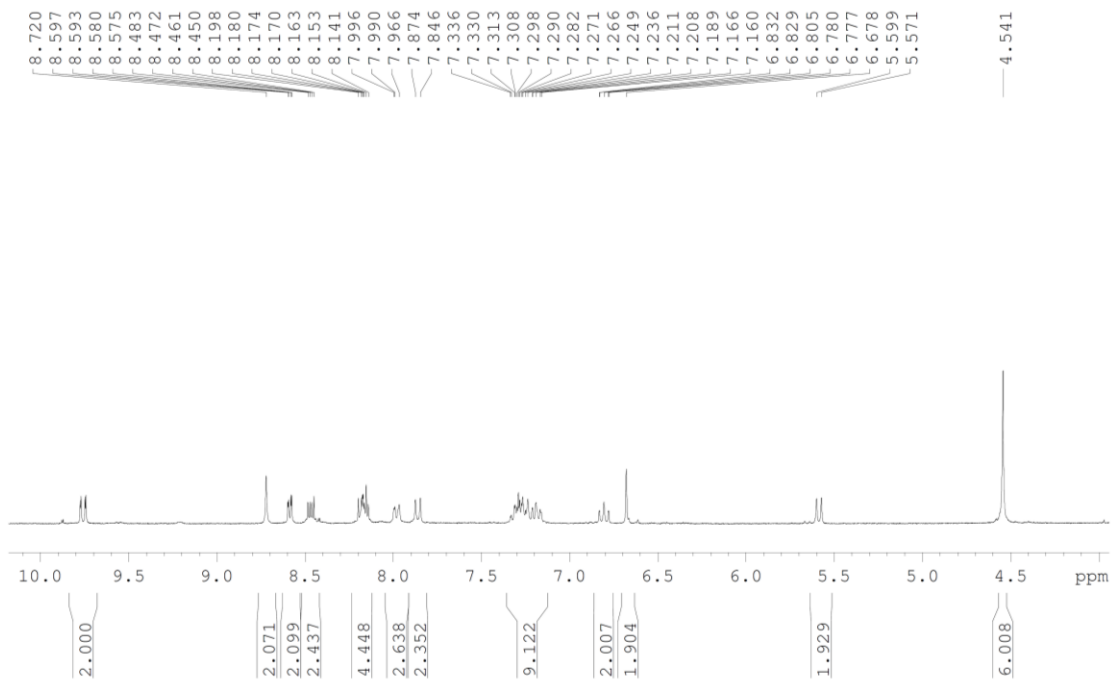


**Figure S4**. $^1$H NMR in DMSO-$d_6$ for **2b**.
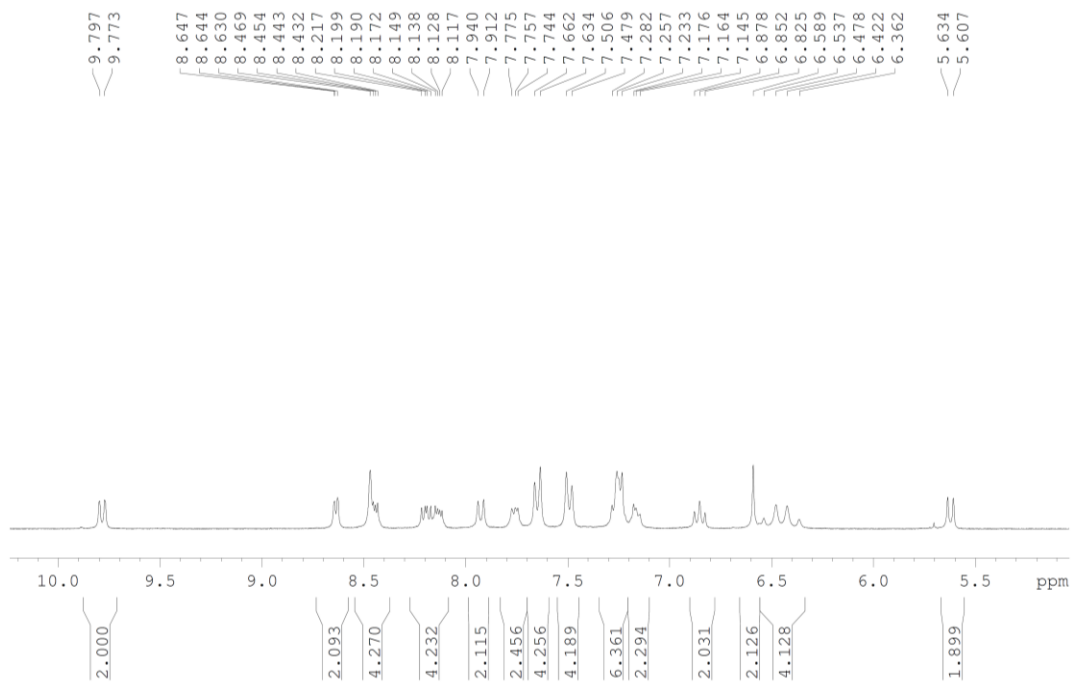
**Figure S5**. $^{1}$H NMR in DMSO-d$_6$ for **2c**.
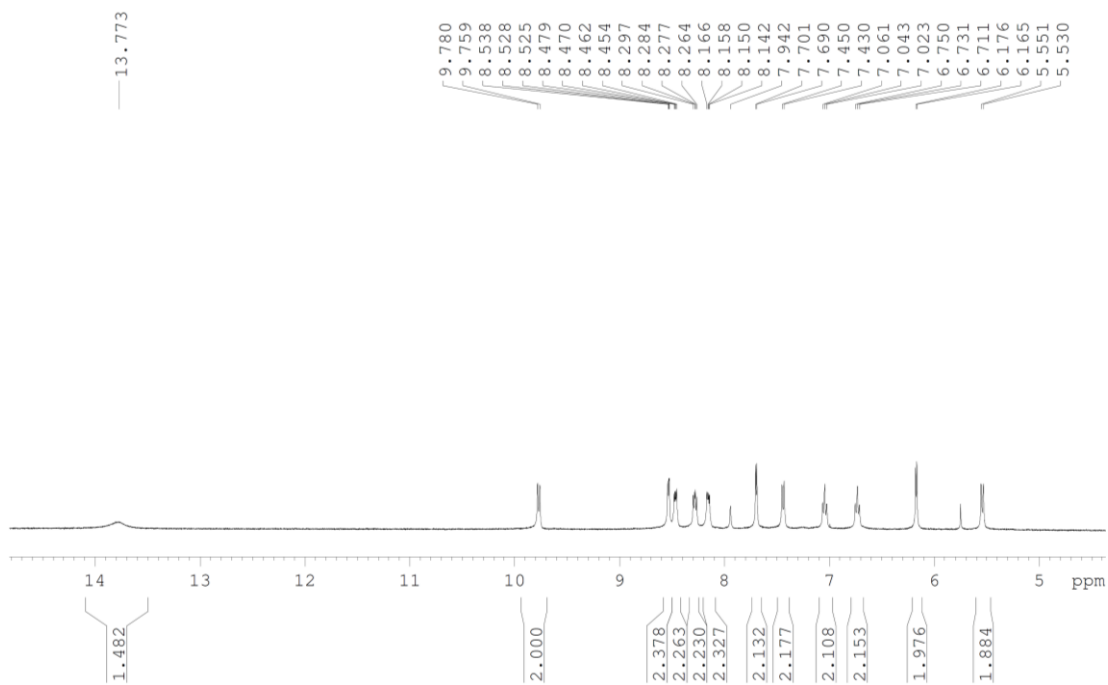
**Figure S6**. $^1$H NMR in DMSO-d$_6$ for **3a**.
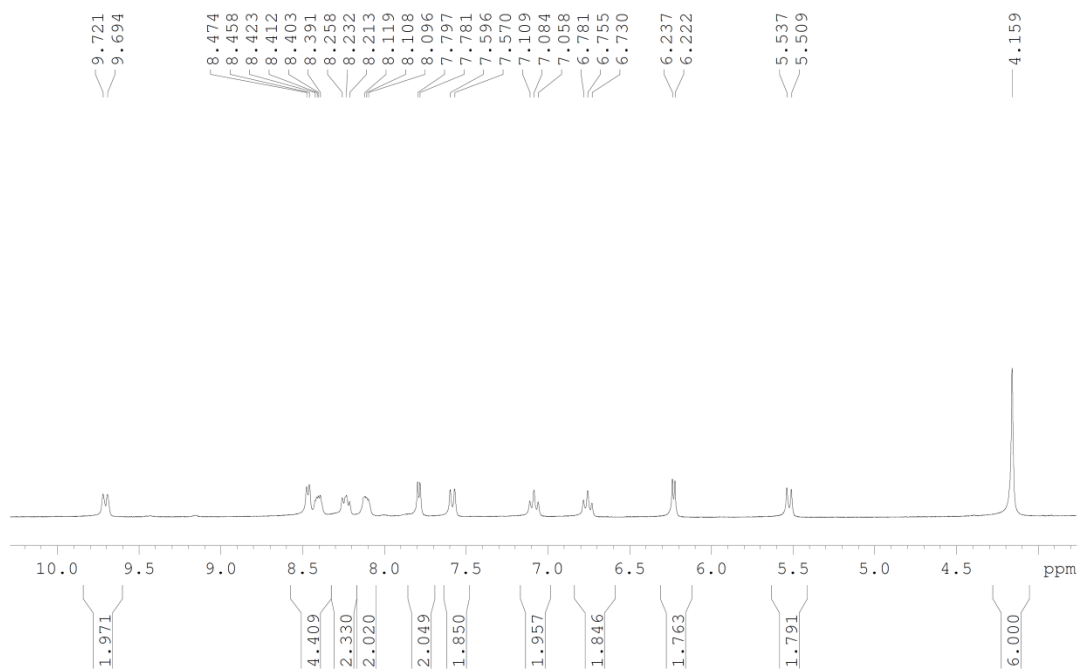


**Figure S7**. $^1$H NMR in DMSO-d$_6$ for **3b**.
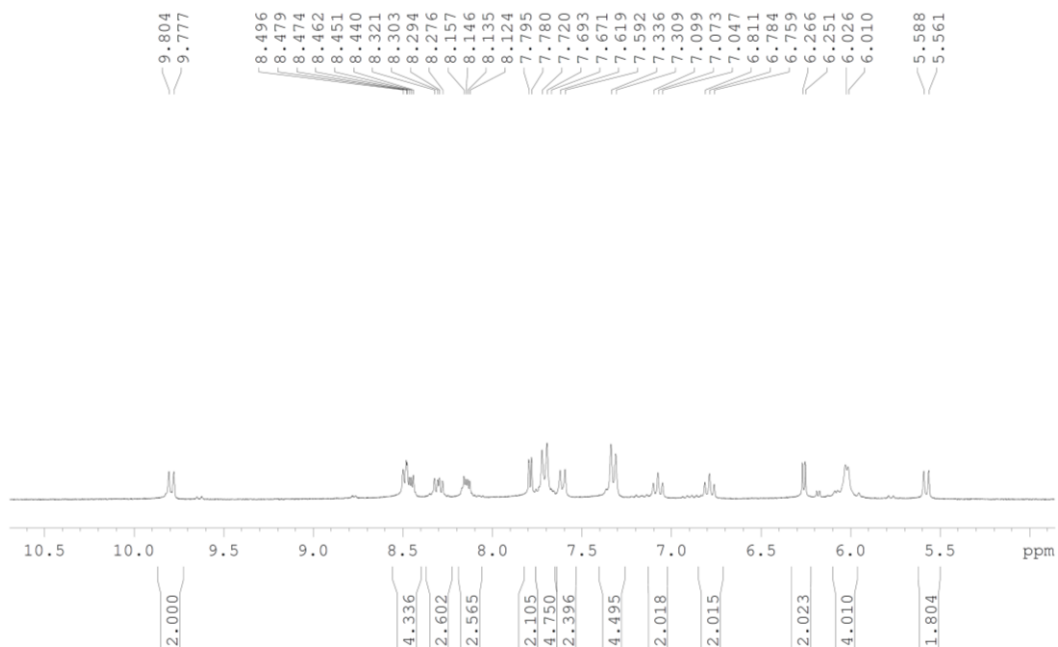
**Figure S8**. $^1$H NMR in DMSO-d$_6$ for **3c**.

**(RP)HPLC purity and stability analyses.** The purity of Ir(III) complexes was analyzed using an (RP)HPLC/MS TOF 6220 equipped with a double binary pump (model G1312A), degasser, autosampler (model G1329A), diode array detector (model G1315D) and mass detector in series Agilent Technologies 1200. Chromatographic analyses were carried out on a Brisa C18 column (150 mm × 4.6 mm, 5 μm particle size); Teknokroma, Macclesfield, UK. The mobile phase was a mixture of (A) H$_2$O/HCOOH 0.1% and (B) acetonitrile/HCOOH 0.1%. The flow rate was 0.8 mL/min in a linear gradient starting (see Table S1 in the Supporting Information for the gradient used). Chromatograms were recorded at 280 nm. The HPLC system was controlled by a ChemStation software (MASS HUNTER.). The mass detector was an ion trap spectrometer equipped with a dual source electrospray-APCI. Mass spectrometry data were acquired in the positive ionization mode. The ionization conditions were adjusted at 350 °C and 3 kV for capillary temperature and voltage, respectively. The nebulizer pressure and flow rate of nitrogen were 60 psi and 12 L/min, respectively. The full scan mass covered the range from m/z 100 up to m/z 1000. Samples were dissolved in acetonitrile, DMSO or DMSO/RPMI (50 μM final concentration).

**Table S1**. HPLC method

| Time (min) | 0.1% formic acid in dH$_2$O | 0.1% formic acid in CH$_3$CN |
| --- | --- | --- |
| 0-14 | 90 | 10 |
| 14-19.5 | 10 | 90 |
| 19.6-24 | 90 | 10 |

10
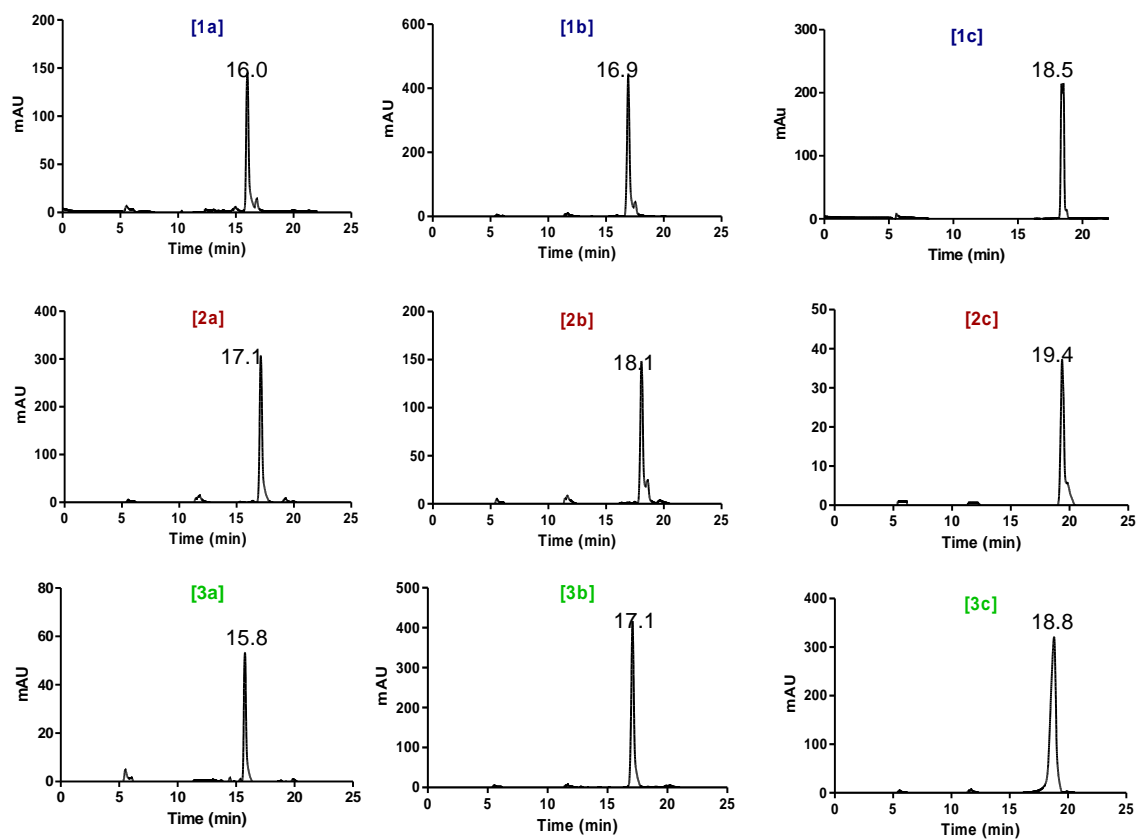
**Figure S9.** HPLC chromatograms of **1a-c**, **2a-c** and **3a-c** in DMSO.
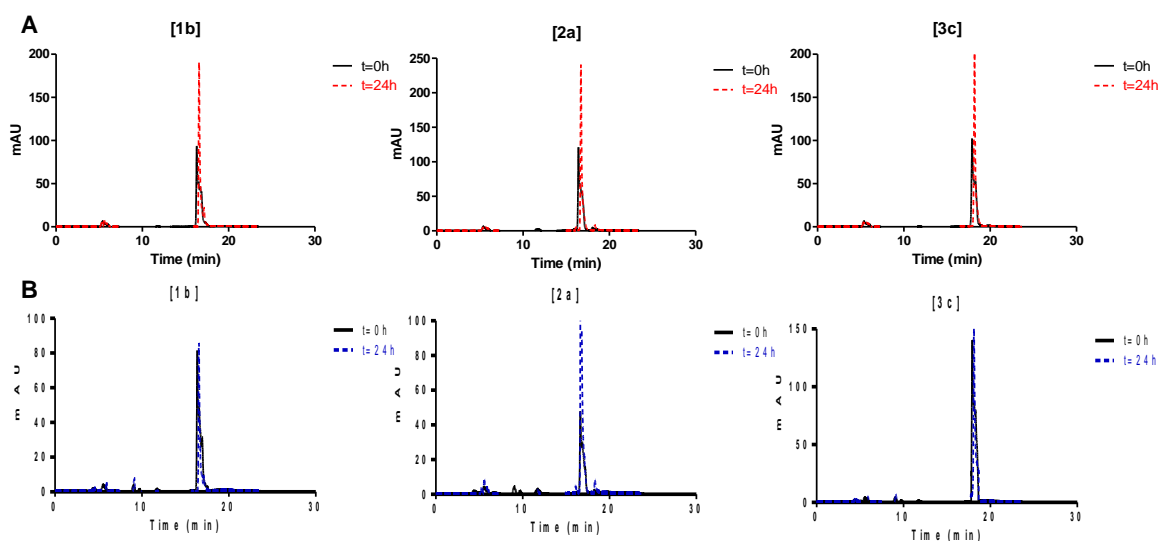


**Figure S10**. HPLC chromatograms of complexes **1b**, **2a** and **3c** in A) DMSO at t= 0 h (—) and t= 24 h (– –) incubation and B) RPMI culture medium (contain 5% DMSO) at t= 0 h (—) and t= 24 h (– –) incubation.

**Details of measurements of UV/Vis absorption and luminescence spectra.** UV/Vis spectroscopy was carried out on a PerkinElmer Lambda 750 S spectrometer with operating software, and emission spectra were obtained with a Horiba Jobin Yvon Fluorolog 3−22 modular spectrofluorometer with a 450 W xenon lamp. Measurements were performed in a right angle configuration using 10 mm quartz fluorescence cells for solutions at 298 K. Emission lifetimes ($\tau$) were measured using an IBH FluoroHub TCSPC controller and a NanoLED pulse diode excitation source ($\tau < 10\mu s$); the estimated uncertainty is ±10% or better. Emission quantum yields ($\Phi$) were measured using a Hamamatsu C11347 Absolute PL Quantum Yield Spectrometer; the estimated uncertainty is ±5% or better. $H_2O$/DMSO (99:1) solutions of the samples were previously degassed by bubbling argon for 30 min. Emission spectra of **1a**, **2a** and **3a** were recorded in aerated disodium hydrogen phosphate/citric acid buffer solutions (pH 3.3, 5.4. 6.3 and 7.4).
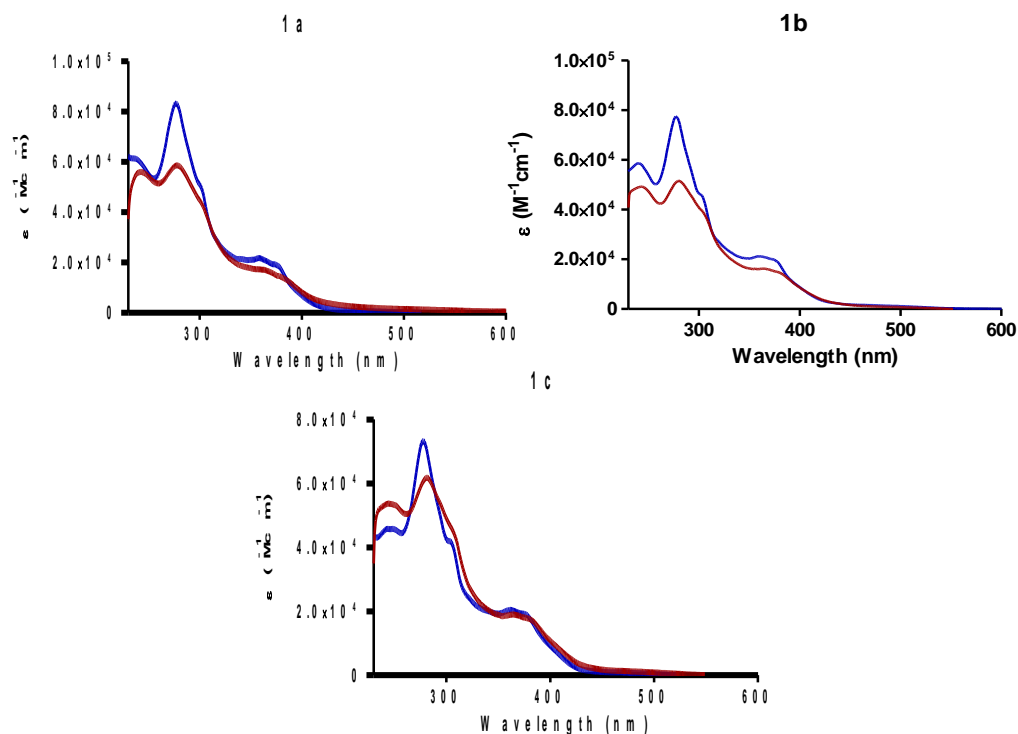


**Figure S11**. UV/Vis absorption spectra of complexes **1a–c** in acetonitrile (blue) and $H_2O$/DMSO (99:1) (red) at room temperature.
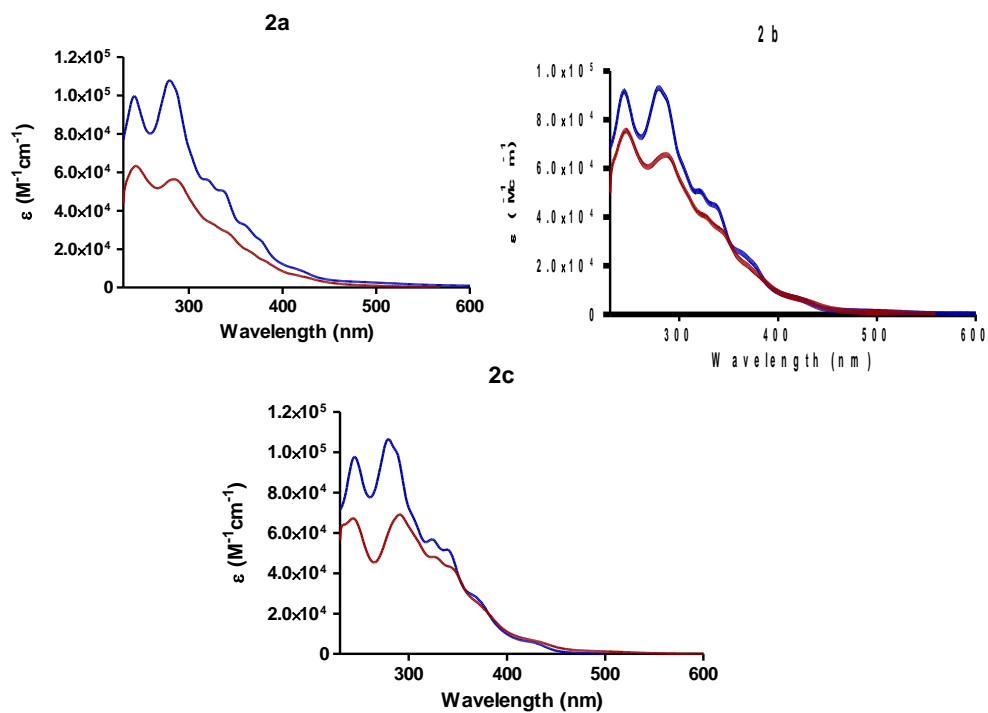
**Figure S12**. UV/Vis absorption spectra of complexes **2a–c** in acetonitrile (blue) and H₂O/DMSO (99:1) (red) at room temperature.
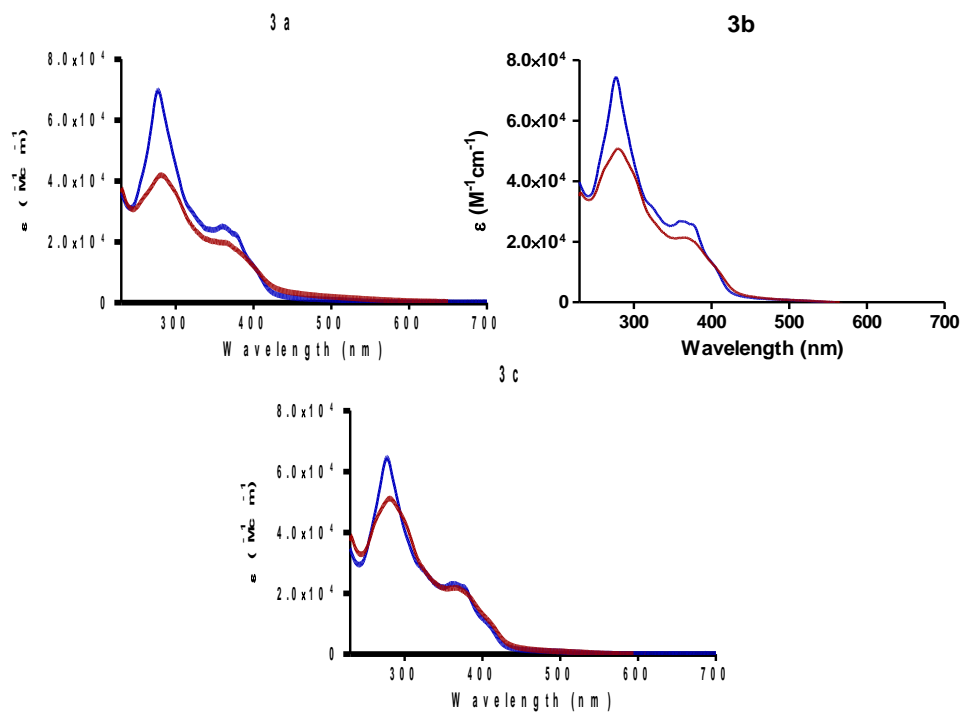


**Figure S13**. UV/Vis absorption spectra of complexes **3a–c** in acetonitrile (blue) and H₂O/DMSO (99:1) (red) at room temperature.
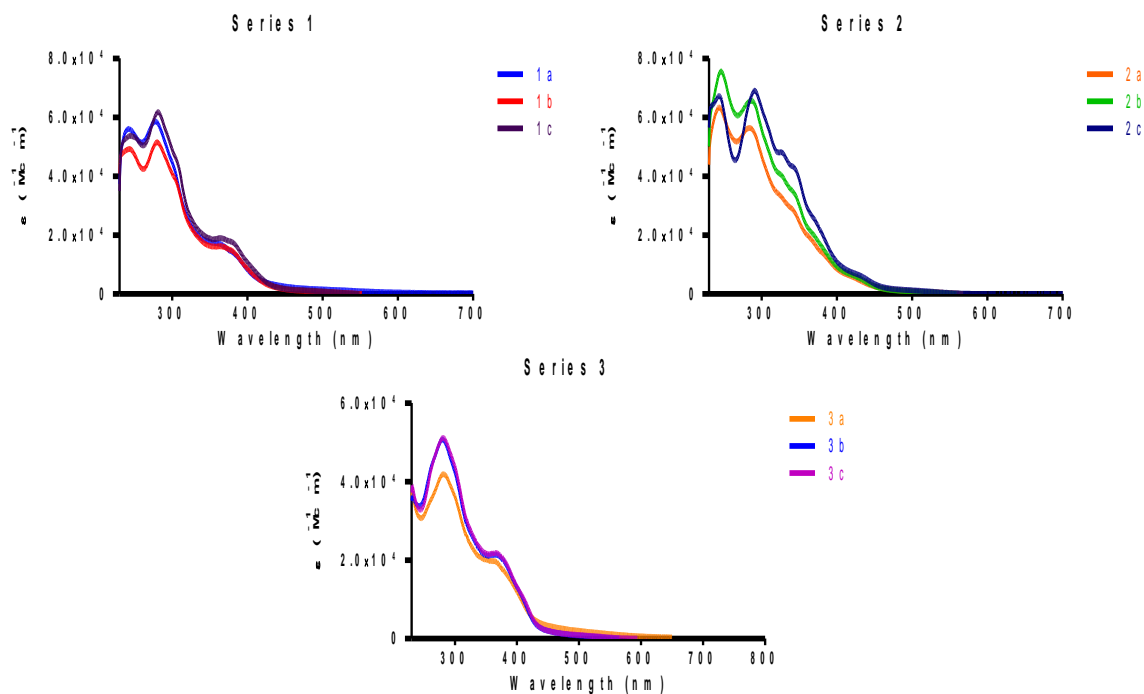
**Figure S14**. Comparison of UV/Vis absorption spectra of complexes **1a–c**, **2a–c** and **3a–c** in H₂O/DMSO (99:1).

**Table S2**. UV/Vis absorption bands and extinction coefficients for **1a–3c** in H₂O/DMSO solution.

| Compound | Wavelength, nm ($\varepsilon$ average, M$^{-1}$ cm$^{-1}$) | | | | |
|---|---|---|---|---|---|
| **1a** | 246 (55540) | 282 (57550) | 369 (16240) | 385 (13100) | 426 (3850) |
| **1b** | 248 (48230) | 285 (50020) | 369 (15970) | 381 (14440) | 429 (2930) |
| **1c** | 245 (54130) | 281 (61820) | 370 (18640) | 380 (17773) | 425 (4220) |
| **2a** | 247 (62220) | 288 (55779) | 342 (28407) | 385 (12790) | 432 (4500) |
| **2b** | 249 (74540) | 291 (64490) | 347 (32340) | 400 (9340) | 436 (4530) |
| **2c** | 247 (65670) | 294 (67910) | 345 (42340) | 380 (20690) | 436 (5590) |
| **3a** | 286 (41550) | 369 (19020) | 380 (16830) | 429 (4790) | |
| **3b** | 285 (49690) | 372 (20980) | 390 (16610) | 431 (3520) | |
| **3c** | 284 (50750) | 375 (20690) | 385 (18220) | 428 (4450) | |

**Figure S15**. Fluorescence emission decay kinetics of series 1 in $H_2O$/DMSO solution.
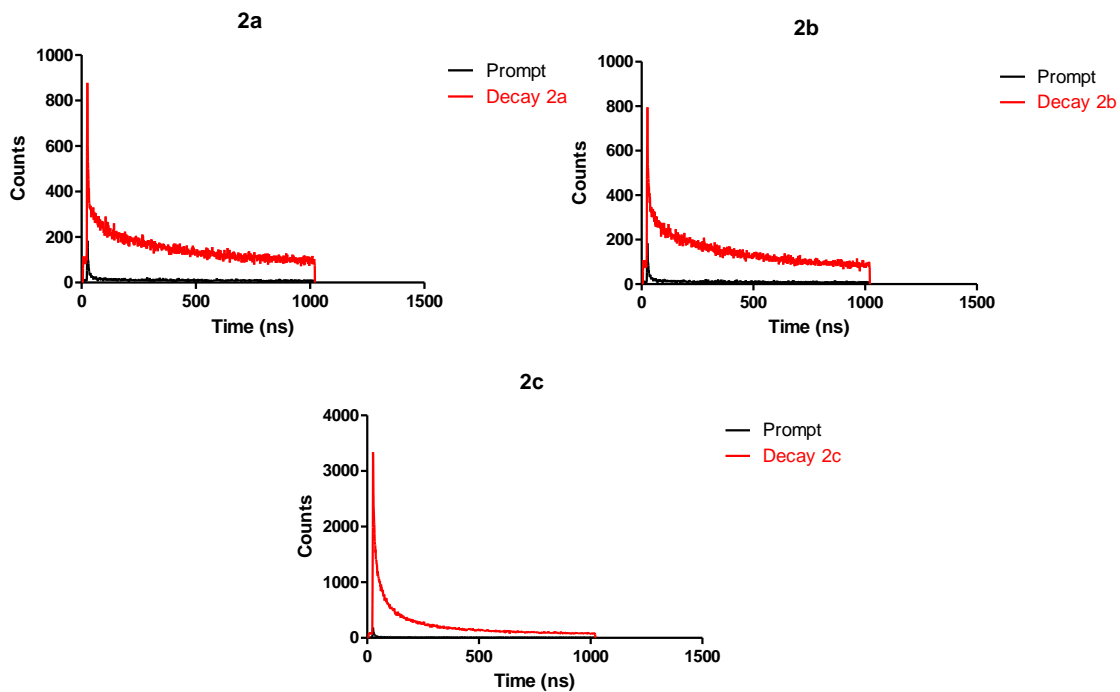


**Figure S16**. Fluorescence emission decay kinetics of series 2 in $H_2O$/DMSO solution.
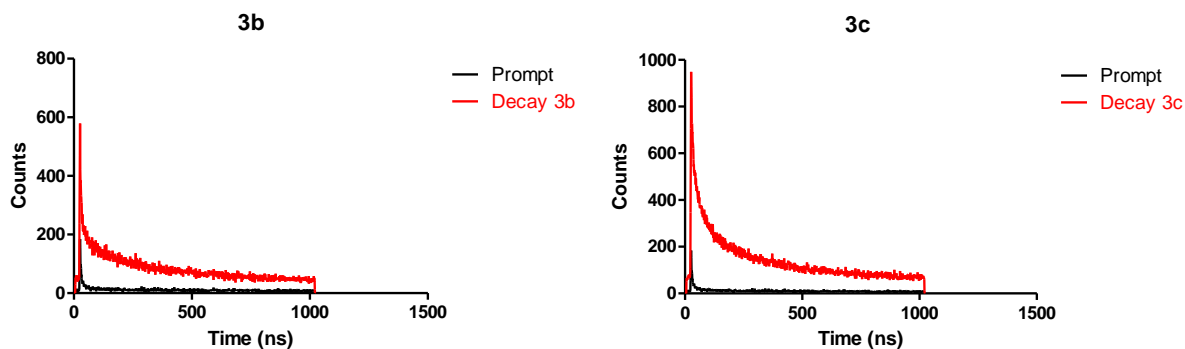
**Figure S17**. Fluorescence emission decay kinetics of series 3 in $H_2O$/DMSO solution.
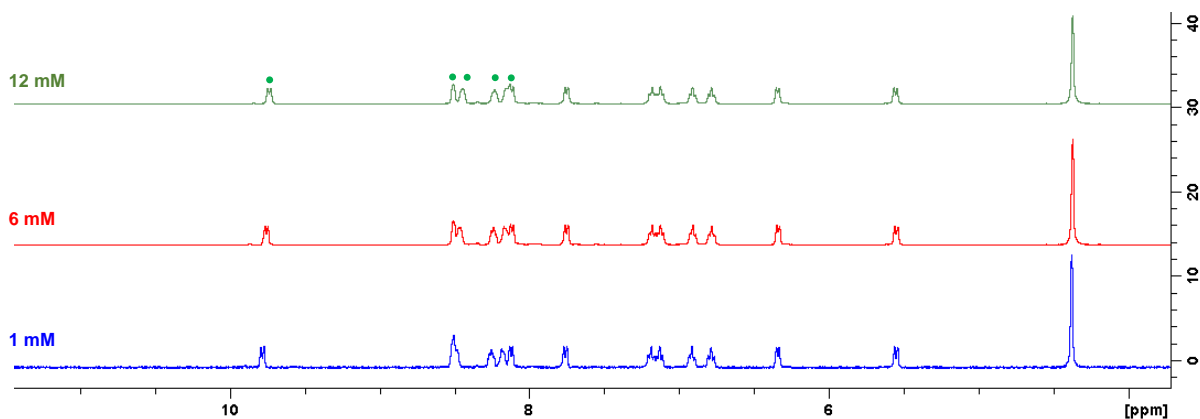


**Figure S18**. $^1H$ NMR spectral traces of **1b** at different concentration in DMSO-$d_6$ (400 MHz, 298 K). Some proton signals of dppz ligand show an upfield shift when the concentration increases.
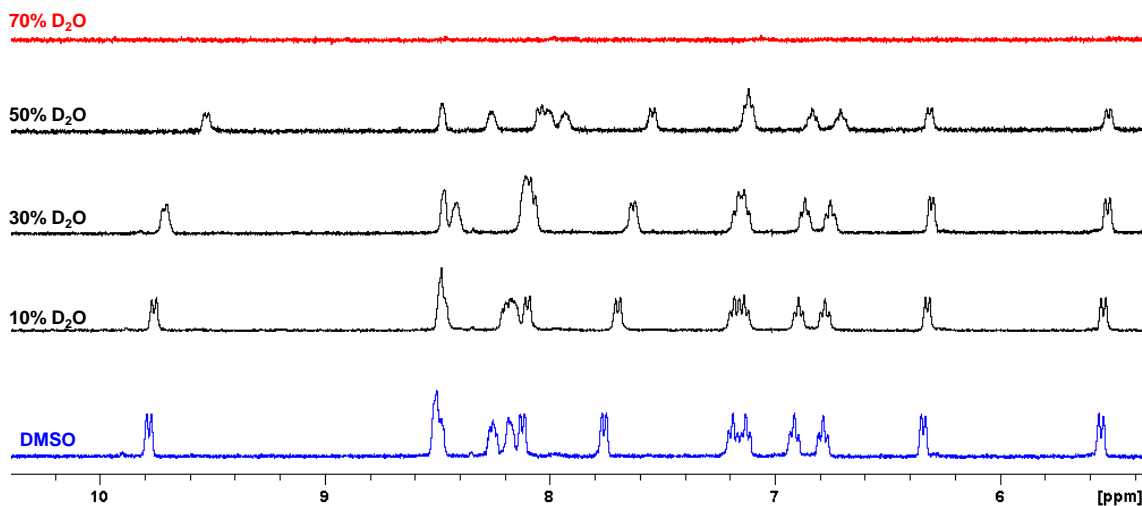


**Figure S19**. $^1H$ NMR spectral traces of **1b** at different composition of $D_2O$ in DMSO-$d_6$ (1 x $10^{-3}$ M, 400 MHz, 298 K). The proton signals show an upfield shift when the percentage of

water increases from 0 to 30%, indicating the occurrence of aggregation. The increase of the water content up to 70% gives as broad signals that lead to the virtual disappearance of spectra.
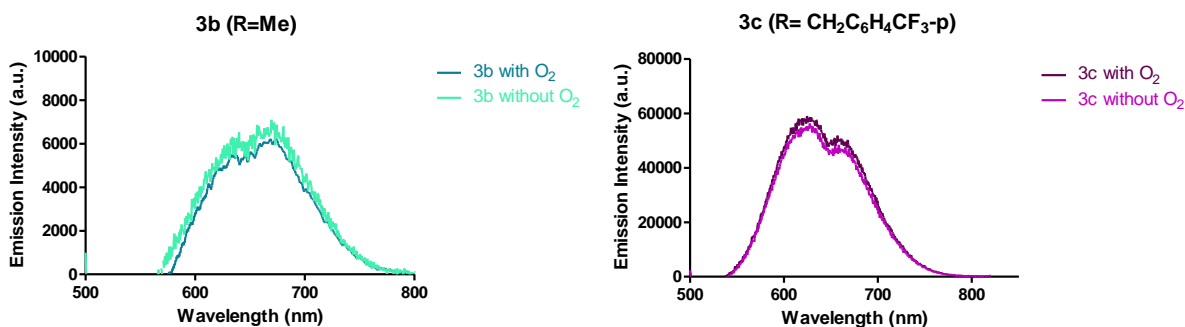


**Figure S20**. Emission spectra of **3b** and **3c** in aerated and deaerated $H_2O$/DMSO (99:1), 10 µM. λexc= 420 nm.
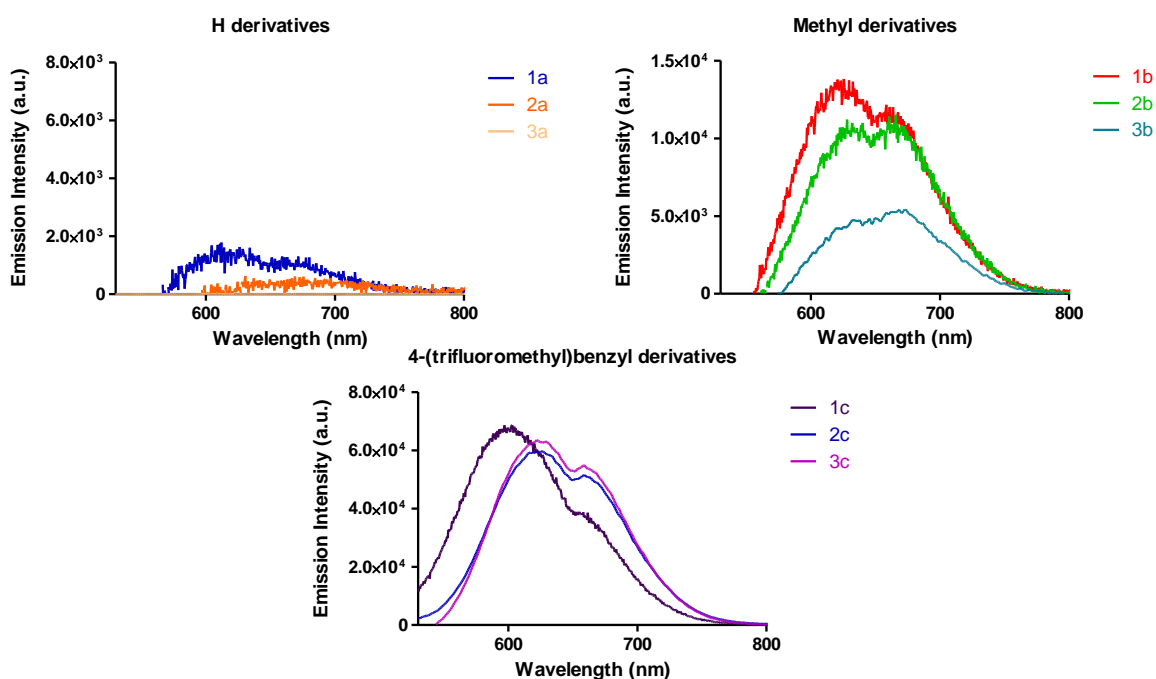


**Figure S21.** Effect of substituent in the emission of Ir complexes in $H_2O$/DMSO (99:1), 10 µM. λexc= 420 nm.
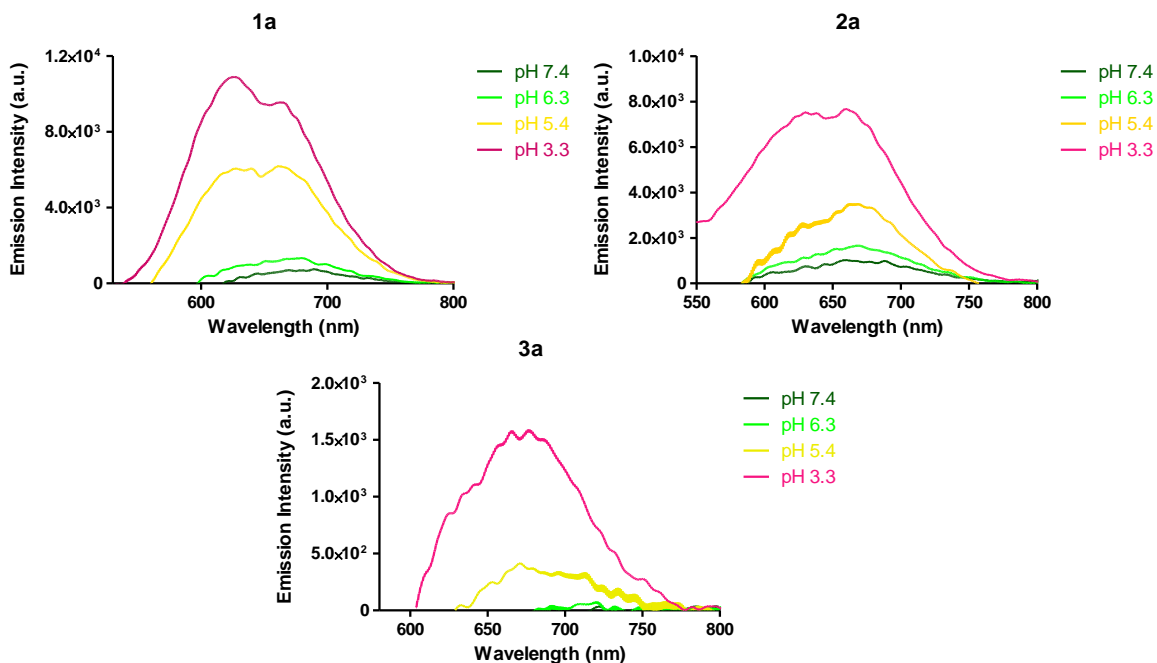
**Figure S22.** pH-sensitive emission of complexes **1a**, **2a** and **3a** in buffer/DMSO (99:1), 10 µM. λexc= 420 nm.
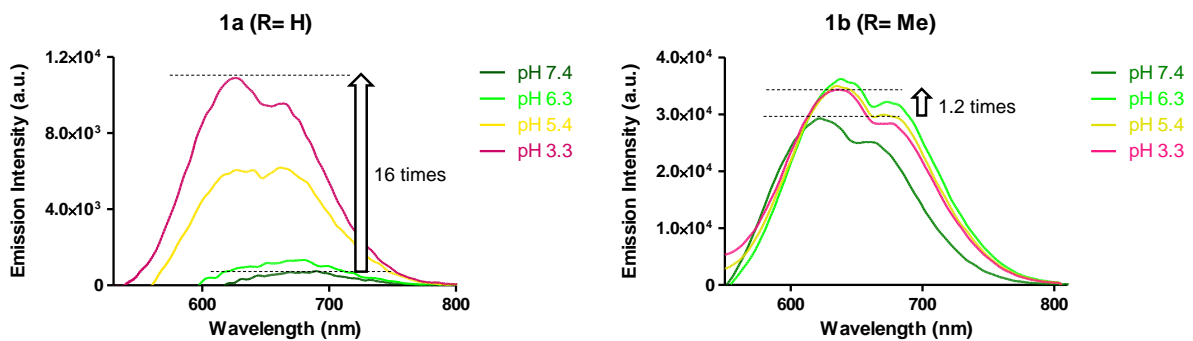


**Figure S23**. pH dependence on the luminescence for **1a** and **1b** in buffer/DMSO (99:1).
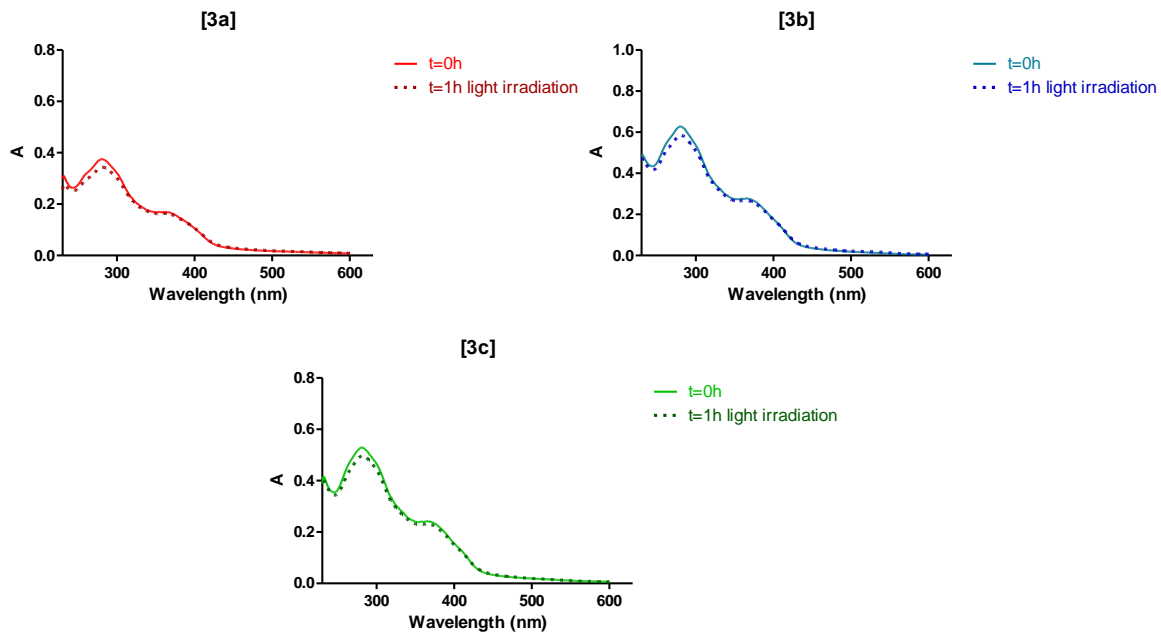
**Figure S24**. Photostability of complexes **3a–c** in H$_2$O/DMSO at 450 nm.

**Table S3.** Crystal data for **2b**.

| $C_{54}H_{36}IrN_8 \cdot 0.5(C_{7.28}H_{6.56}Cl_{3.28}) \cdot F_6P \cdot 2.18(C_2H_4Cl_2)$ | $Z = 2$ |
|---|---|
| $M_r = 1454.95$ | $F(000) = 1448$ |
| Triclinic, $P\bar{1}$ | $D_x = 1.595$ Mg m$^{-3}$ |
| $a = 14.2342$ (14) Å | Mo $K\alpha$ radiation, $\lambda = 0.71073$ Å |
| $b = 15.3701$ (15) Å | Cell parameters from 9790 reflections |
| $c = 15.5819$ (15) Å | $\theta = 2.3–29.6°$ |
| $\alpha = 65.102$ (3)° | $\mu = 2.56$ mm$^{-1}$ |
| $\beta = 83.431$ (3)° | $T = 100$ K |
| $\gamma = 78.541$ (3)° | Block, orange |
| $V = 3028.7$ (5) Å$^3$ | $0.29 \times 0.20 \times 0.13$ mm |

**Table S4.** Data collection for **2b**.

| Bruker D8 Quest CCD diffractometer | 11041 reflections with $I > 2\sigma(I)$ |
|---|---|
| Radiation source: fine-focus sealed tube | $R_{int} = 0.032$ |
| $\omega$ and $\phi$ scans | $\theta_{max} = 25.6°$, $\theta_{min} = 1.9°$ |
| Absorption correction: multi-scan (*SADABS*; Sheldrick, 1996) | $h = -17 \rightarrow 17$ |
| $T_{min} = 0.610$, $T_{max} = 0.746$ | $k = -18 \rightarrow 18$ |
| 330048 measured reflections | $l = -18 \rightarrow 18$ |
| 11401 independent reflections | |

**Table S5.** Refinement data for **2b**.

| | |
|---|---|
| Refinement on $F^2$ | 0 restraints |
| Least-squares matrix: full | Hydrogen site location: inferred from neighbouring sites |
| $R[F^2 > 2\sigma(F^2)] = 0.0412$ <br> $wR[F^2 > 2\sigma(F^2)] = 0.1123$ | H-atom parameters constrained |
| $R(F^2) = 0.0424$ <br> $wR(F^2) = 0.1133$ | $w = 1/[\sigma^2(F_o^2) + (0.0609P)^2 + 17.7437P]$ <br> where $P = (F_o^2 + 2F_c^2)/3$ |
| $S = 1.08$ | $(\Delta/\sigma)_{max} = 0.001$ |
| 11401 reflections | $\Delta\rangle_{max} = 3.24$ e Å$^{-3}$ |
| 774 parameters | $\Delta\rangle_{min} = -1.27$ e Å$^{-3}$ |
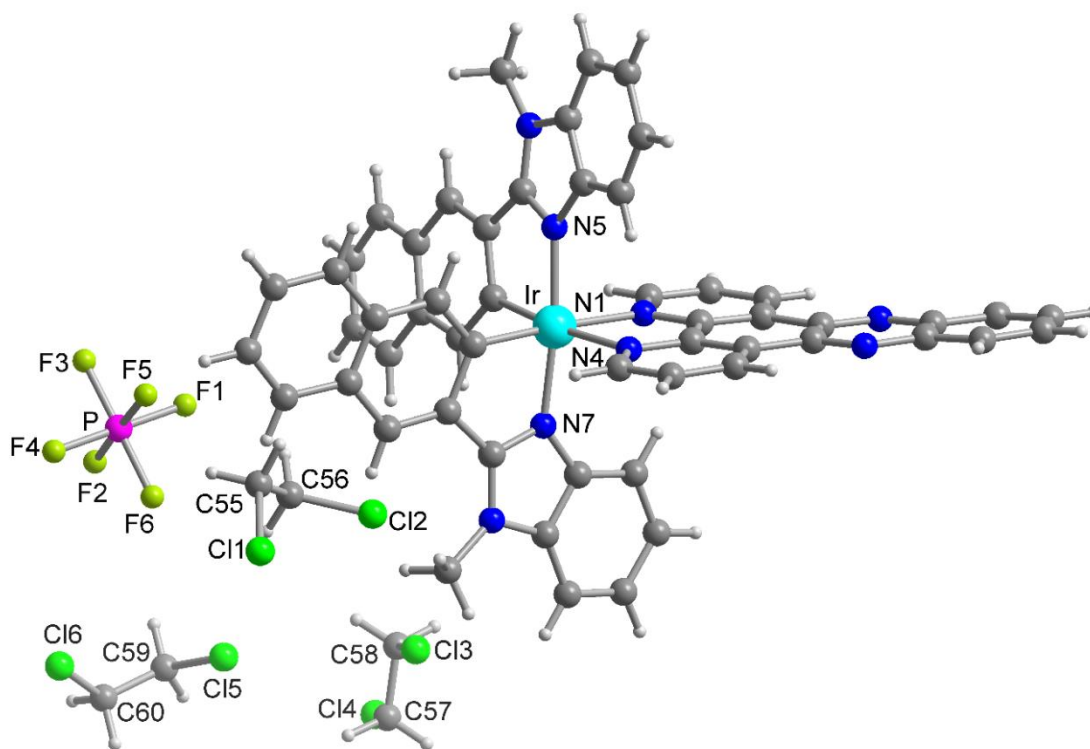
**Figure. S25.** Molecular structure within the crystal of **2b**, (showing the iridium cation, the PF$_6$ anion and three 1,2-dichloroethane solvent molecules of crystallization. The disordered hexane and site-sharing C$_2$H$_4$Cl$_4$ molecule were not shown for clarity.

**Table S6** C-H⋯F Hydrogen-bond geometry (Å, °) for **2b**.[a]

```
================================================================================
Analysis of Potential Hydrogen Bonds and Schemes with d(D...A) < R(D)+R(A)+0.50, d(H...A) < R(H)+R(A)-
0.12 Ang., D-H...A > 100.0 Deg
================================================================================
Note: - ARU codes in [] are with reference to the Coordinates printed above (Possibly transformed, when MOVE
.NE. 1.555)
================================================================================
```

| D --- H....A | [ ARU ] | D - H | H...A | D...A | D - H...A |
|---|---|---|---|---|---|
| C(15) --H(15) ..F(3) | [ 1556.03] | 0.95 | 2.50 | 3.437(7) | 167 |
| C(22) --H(22) ..F(1) | [ 2566.03] | 0.95 | 2.50 | 3.280(8) | 139 |
| C(22) --H(22) ..F(3) | [ 2566.03] | 0.95 | 2.53 | 3.251(8) | 133 |
| C(41) --H(41) ..F(4) | [ 2656.03] | 0.95 | 2.38 | 3.228(8) | 148 |
| C(49) --H(49) ..F(4) | [ 2556.03] | 0.95 | 2.44 | 3.141(8) | 130 |
| C(54) --H(54C) ..F(2) | [ 2656.03] | 0.98 | 2.48 | 3.418(8) | 161 |
| C(55) --H(55A) ..F(5) | [ 1555.03] | 0.99 | 2.41 | 3.247(12) | 141 |
| C(55) --H(55A) ..F(6) | [ 1555.03] | 0.99 | 2.55 | 3.203(14) | 124 |
| C(56) --H(56B) ..F(6) | [ 1555.03] | 0.99 | 2.50 | 2.990(13) | 110 |
| C(57) --H(57B) ..F(3) | [ 1655.03] | 0.99 | 2.50 | 3.355(13) | 145 |

```
[ 2566.] = [  2_566] = -x, 1-y, 1-z
[ 2656.] = [  2_656] = 1-x, -y, 1-z
[ 2556.] = [  2_556] = -x, -y, 1-z
[ 1556.] = [  1_556] = x, y, 1+z
[ 1655.] = [  1_655] = 1+x, y, z
```

[a] D = Donor, A = Acceptor. For found and refined H atoms the standard deviations are given for their hydrogen bond distances and angles.

**Table S7.** Analysis of *inter*molecular C-H...Cg(Pi-Ring) Interactions (H..Cg < 3.0 Ang. - Gamma < 30.0 Deg) in **2b** (see Scheme S6 for explanation).

- Cg(J)  = Center of gravity of ring J (Plane number above)
- H-Perp  = Perpendicular distance of H to ring plane J
- Gamma   = Angle between Cg-H vector and ring J normal
- C-H..Cg = C-H-Cg angle (degrees)
- C..Cg   = Distance of X to Cg (Angstrom)
- C-H, Pi = Angle of the X-H bond with the Pi-plane (i.e.' Perpendicular = 90 degrees, Parallel = 0 degrees)

| C--H(I)   Cg(J) [   ARU(J)] | H..Cg | H-Perp | Gamma | C-H..Cg | C..Cg | C-H,Pi |
|---|---|---|---|---|---|---|
| C(9)-H(9) -> Cg(14) [ 2667.01] | 2.83 | 2.75 | 13.39 | 155 | 3.710(7) | 69 |
| C(36)-H(36C) -> Cg(12) [ 2566.01] | 2.77 | 2.65 | 16.91 | 127 | 3.448(6) | 52 |
| C(39)-H(39) -> Cg(12) [ 2666.01] | 2.85 | 2.57 | 25.83 | 152 | 3.718(6) | 88 |
| C(39)-H(39) -> Cg(13) [ 2666.01] | 2.78 | 2.57 | 22.61 | 156 | 3.670(7) | 89 |

[  2667] = 1-X,1-Y,2-Z
[  2566] = -X,1-Y,1-Z
[  2666] = 1-X,1-Y,1-Z

The Cg(I) refer to the Ring Centre-of-Gravity numbers given in
Cg(12) = Ring C26-C27-C28-C29-C34-C35
Cg(13) = Ring C29-C30-C31-C32-C33-C34
Cg(14) = Ring C37-C38-C39-C40-C41-C42

Significant intermolecular C-H···π contacts start below around 2.7 Å for the (C-)H···ring centroid distances with H-perp also starting at below 2.6-2.7 Å and C-H··Cg > 145°.[11]
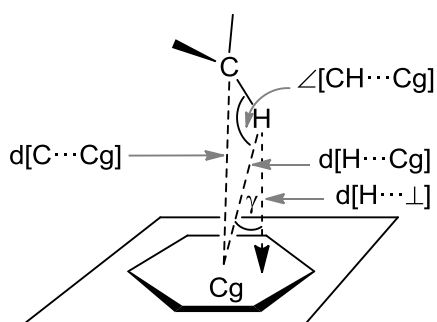


**Scheme S6**. Graphical presentation of the parameters used for the description of CH-π interactions.

**Table S8** Packing Analysis for **2b** for possible π−π interactions (see Scheme S7 for explanation).

```
=================================================================================
Analysis of Short Ring-Interactions with Cg-Cg Distances <  6.0 Angstrom and Beta < 60.0Deg.
=================================================================================
```

- Cg(I)    = Plane number I (= ring number in () above)
- Alpha    = Dihedral Angle between Planes I and J (Deg)
- Beta     = Angle Cg(I)-->Cg(J) or Cg(I)-->Me vector and normal to plane I (Deg)
- Gamma    = Angle Cg(I)-->Cg(J) vector and normal to plane J (Deg)
- Cg-Cg    = Distance between ring Centroids (Ang.)
- CgI_Perp = Perpendicular distance of Cg(I) on ring J (Ang.)
- CgJ_Perp = Perpendicular distance of Cg(J) on ring I (Ang.)
- Slippage = Distance between Cg(I) and Perpendicular Projection of Cg(J) on Ring I (Ang).

| Cg(I) Res(I)  Cg(J) [  ARU(J)] | Cg-Cg | Alpha | Beta | Gamma | CgI_Perp | CgJ_Perp | slippage |
|---|---|---|---|---|---|---|---|
| Cg(8)  [ 1] -> Cg(10) [ 2667.01] | 3.796(3) | 5.1(3) | 26.5 | 23.6 | 3.479(2) | 3.398(3) | 1.692 |
| Cg(10) [ 1] -> Cg(8)  [ 2667.01] | 3.796(3) | 5.1(3) | 23.6 | 26.5 | 3.398(3) | 3.479(2) | 1.517 |
| Cg(10) [ 1] -> Cg(22) [ 2667.01] | 3.898(3) | 4.7(2) | 25.3 | 30.0 | 3.375(2) | 3.5224(14) | 1.668 |
| Cg(22) [ 1] -> Cg(10) [ 2667.01] | 3.897(3) | 4.7(2) | 30.0 | 25.3 | 3.5224(14) | 3.375(2) | 1.950 |

[  2667] = 1-X,1-Y,2-Z
Cg8 = centroid of ring N4-C13-C14-C15-C16-C18
Cg10 = centroid of ring C6-C7-C8-C9-C10-C11
Cg22 = centroid of ring N4-C4-C5-C12-C13-C14-C15-C16-C17-C18

The PLATON-listing **"Analysis of Short Ring-Interactions" for possible π-stacking interactions** yielded mainly rather long centroid-centroid distances (>4.0 Å) together with non-parallel ring planes (alpha >> 0°) and large slip angles (β, γ >30°).

In comparison, significant π-stacking show rather short centroid-centroid contacts (<3.8 Å), near parallel ring planes (alpha < 10° to ~0° or even exactly 0° by symmetry), small slip angles (β, γ <25°) and vertical displacements (slippage <1.5 Å) which translate into a sizable overlap of the aryl-plane areas.[12]

π-Interactions between pyridyl-type ligands for comparison:[13]
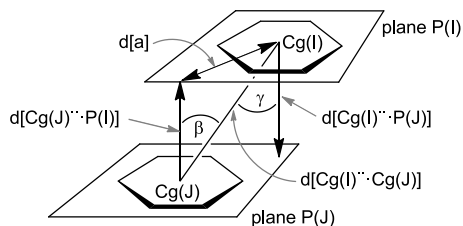


**Scheme S7**. Graphical presentation of the parameters used for the description of π−π stacking.[12]

**Antiproliferative and phototoxicity testing**. The phototoxic activity of Ir complexes was determined against human cervix adenocarcinoma (HeLa) cells obtained from ECACC in the same way as described in several previously published articles.[14] Cells were seeded on 96-well tissue culture plates at a density of $5 \times 10^3$ cells/well in 100 µL of growth medium (DMEM (high glucose, 4.5 $gL^{-1}$) supplemented with gentamycin (50 $mgmL^{-1}$) and 10% heat-inactivated fetal bovine serum) and left to adhere at 37 °C in a humidified 5% $CO_2$ atmosphere for 1 h. After washing cells with PBS, the tested compound was added in EBSS and incubated for 1 h under cultivation conditions. After the incubation period, cells were irradiated for 1 h ($\lambda_{max}$ = 420 nm, $77 \pm 3$ W $m^{-2}$) in the presence of the investigated Ir compound. Subsequently, EBSS with compound was removed, cells were washed with PBS, and then returned to the incubator in complete DMEM medium. Nonirradiated controls were tested as well. The stock solutions of compounds were always freshly prepared in DMSO before use. The final concentration of DMSO in the cell culture medium did not exceed 0.1% (v/v), which was shown not to affect cell growth. The metabolic activity of the cells was determined 70 h after irradiation using standard MTT assay. Briefly, 10 µL of MTT solution (5 mg $mL^{-1}$) was added to each well, and plates were incubated for 4 h. At the end of the incubation time, the medium was removed, and the formazan product was dissolved in 100 µL of DMSO per well. Cell viability was evaluated by measuring the absorbance at 570 nm (reference wavelength at 630 nm) using an absorbance reader Synergy Mx (Biotek, USA). The $IC_{50}$ values were calculated from curves constructed by plotting cell survival (%) versus drug concentration (µM). All experiments were done in triplicate. The reading values were converted to the percentage of control (% cell survival). Phototoxic effects were expressed as $IC_{50}$.

**Determination of cellular accumulation.** The HeLa cells were seeded on 100 mm tissue culture dishes ($1.5 \times 10^6$ cells/dish in 8 mL of growth medium). After 48 h of incubation, the cells were treated with tested compounds at final roughly equimolar concentrations (10 µM) for 5 h. The attached cells were harvested by trypsinization, washed twice with cold PBS, counted and pelleted by centrifugation at 300 g, 3 min, 4 °C. The pellets were digested by using high-pressure microwave acid (HCl, 11 M) digestion system (MARS5, CEM) to give a fully homogenized solution. Final iridium or platinum content in the samples was determined by ICP-MS (Agilent technologies, CA, USA).

**Measurements of localization of Ir complexes in cells by confocal microscopy.** HeLa cells were seeded on 35 mm glass bottom confocal culture dishes (Mattek Co., MA, USA) at the density of $1.5 \times 10^5$ cells/dish and incubated overnight. Next day, the cells were treated with the tested compounds **1c**, **2c** and **3c** (5 µM). After the 18 h incubation, cells were co-stained with ER-TrackerTM or MitoTrackerTM (ThermoFisher Scientific, Waltham, MA, USA) and then analyzed on confocal laser-scanning microscope Leica TCS SP8 SMD (Leica microsystems GmbH, Wetzlar, Germany). The investigated Ir complexes were excited at 405 nm. Samples were scanned sequentially, and the emission parameters were carefully set to omit possible fluorescence overlaps. Colocalization analysis was performed as described previously[15] with the use of the Coloc2 plugin in ImageJ software. Briefly, the Pearson coefficient of correlation (PCC) was measured for entire images by default, and the Costes regression method for estimation of the threshold was used. Values of PCC are expressed as the mean ± SDs above the calculated threshold.

**ROS detection.** To determine the oxidative stress human cervix adenocarcinoma cells (HeLa) were seeded on 96-well black plates at a density of 104 cells/well and incubated at 37 °C in a humidified 5% $CO_2$ atmosphere for 16 h (overnight). Subsequently, the cells were treated with the investigated compounds in EBSS at equitoxic concentrations (1, 5, 10 µM) and held under cultivation conditions for 1 h. Then the cells were irradiated with visible light ($\lambda_{max}$= 420 nm) for 1 h. After this irradiation period, intracellular ROS were quantified using a method developed by Robinson et al..[16] Briefly, DCFH-DA (10 µM) was added to cells and samples were incubated for 30 min at 37 °C. The fluorescence intensity was evaluated by measuring the fluorescence (excitation/emission wavelengths: 504 nm/529 nm) using a fluorescence reader Synergy Mx (Biotek, USA).
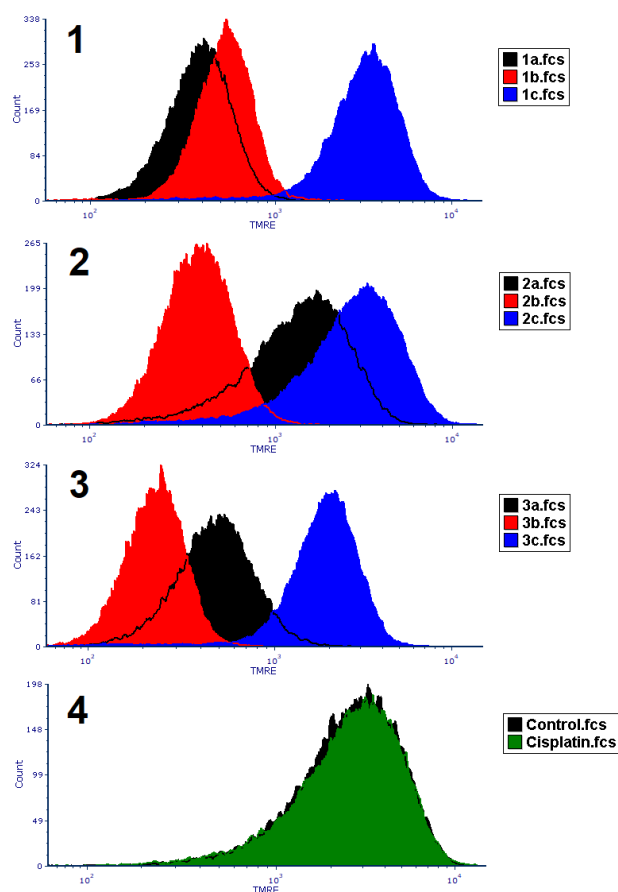


**Figure S26**. Representative overlaid histograms displaying the measurement of mitochondrial membrane potential. HeLa cells were treated with the investigated compounds (10 µM) and incubated for 5 h in the dark. Panels: 1 - Compound 1; 2 – Compounds 2; 3 – Compounds 3; 4 – untreated control (black), cisplatin (green). Colors in panels 1-3 in Figure S20: "a" compounds – black color, "b" – red color, "c" – blue color. Mitochondrial membrane potential was determined by TMRE staining with subsequent analysis by flow cytometry. Histograms are the representatives of two independent experiments, expressed at the bi-exponential scale.
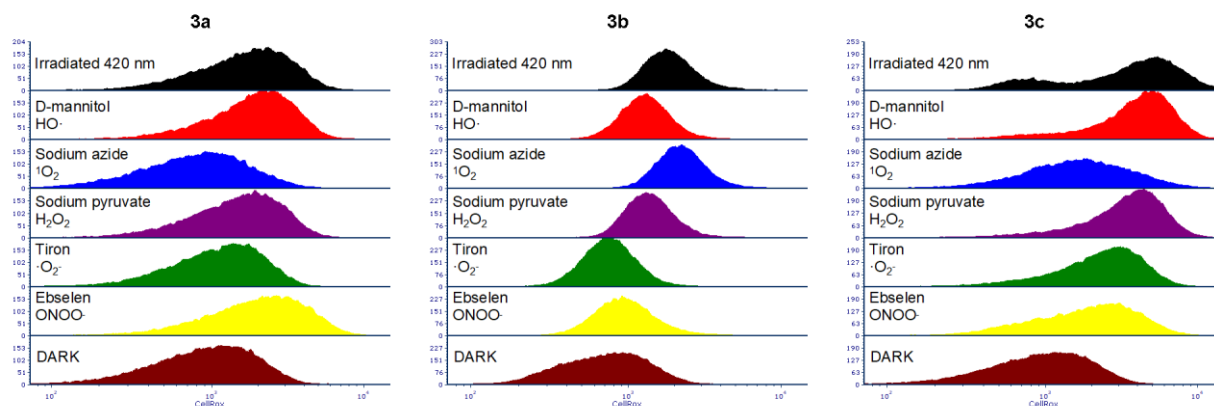
**Figure S27**. Representative histograms displaying determination of ROS in Hela cells treated with 3a-c, as determined by the flow cytometry. Cells were pre-incubated for 1 h with specific ROS scavengers: D-mannitol (50 mM), sodium azide (5 mM), sodium pyruvate (10 mM), tiron (5 mM), and ebselen (50 µM). Cells were treated with the investigated compounds (10 µM), incubated for 1 h in the dark followed by 1 h incubation under the irradiation with 420 nm or 2 h incubation in the dark (samples marked as „dark"). The controls were treated with an appropriate amount of DMSO. Scavengers remained throughout the duration of the whole experiment. Data are the representatives of three independent experiments expressed on the histograms with bi-exponential scale.
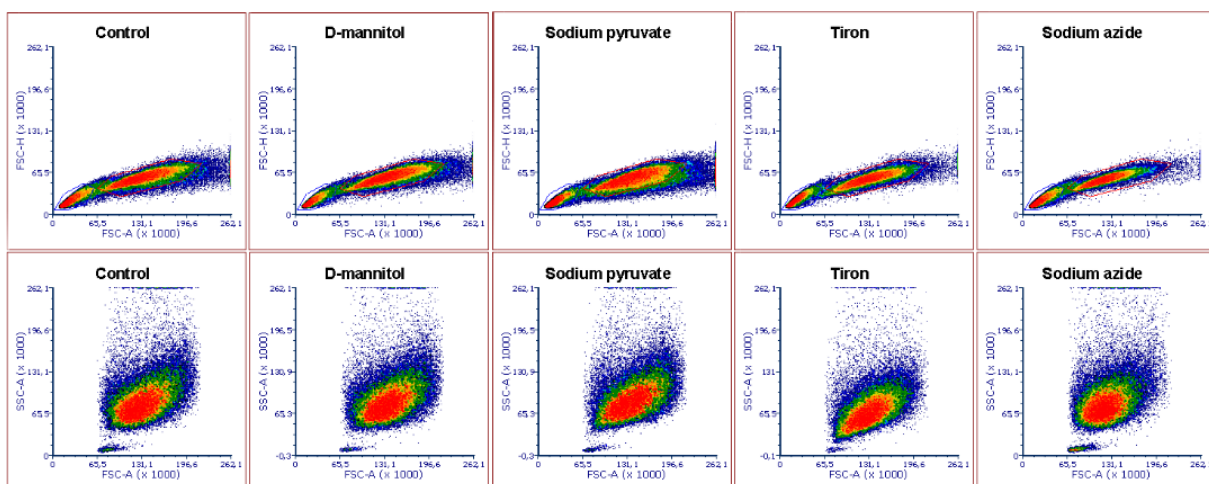


**Figure S28**. Flow cytometric analysis of HeLa cells treated with ROS scavengers. Cells were treated with D-mannitol (50 mM), sodium azide (5 mM), sodium pyruvate (10 mM), tiron (5mM) for 3h to check possible toxic effects of individual scavengers on the cells demonstrated by the number of debris/particles in the sample (top panels) or by cellular granularity (bottom panels). Top panels: forward scatter area vs. forward scatter high; bottom panels: forward scatter area vs. side scatter area.

**Singlet oxygen detection using 1,3-diphenylisobenzofuran (DPBF).** Singlet oxygen was detected by the standard method using DPBF as the $^1O_2$ indicator through monitoring the decrease in the absorption of 1,3-diphenylisobenzofuran (DPBF) due to its photooxidation at 418 nm under blue light irradiation measured by a UV−vis spectrophotometer.[17]
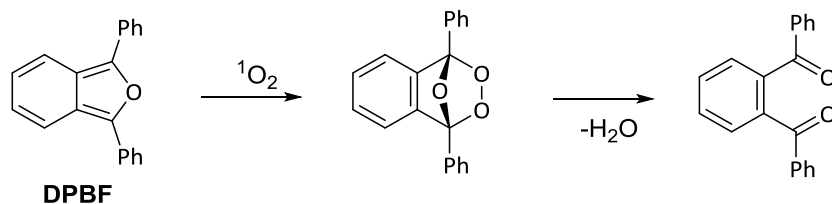


**DPBF**

The PBS solutions (1 % DMSO) of complexes (10 µM) containing 10 µM DPBF, was prepared in the dark and irradiated with blue light (450 nm centered LED). The absorbance of DPBF at 418 nm was recorded every 15 s. A PBS solution (1 % DMSO) of DPBF without the photosensitizer was used as a negative control. The plots shown in Fig. S22 reveal that **3a** and **3c** are efficient $^1O_2$ generators whereas **3b** not, which is consistent with the results demonstrating the involvement of $^1O_2$ in the photopotentiation of Ir-complexes **3a-c** in cells (Fig. 6).
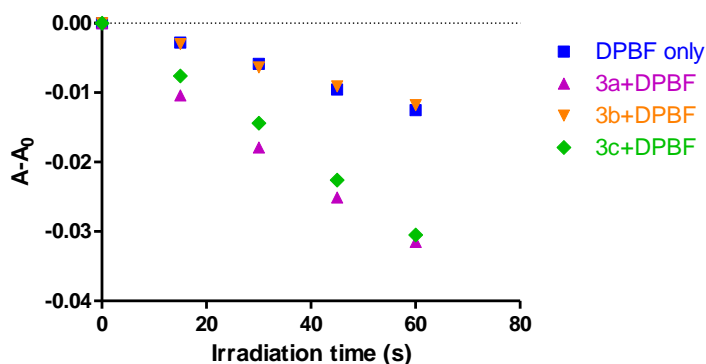


**Figure S29.** Rate of decay of DPBF sensitized by complexes **3a-3c** in PBS solution (1 % DMSO) as shown by the decrease in the absorbance at 418 nm.

**References**

(1) F. Xue, X. Luo, C. Ye, W. Ye and Y. Wang, *Bioorg. Med. Chem.,* 2011, **19**, 2641–2649.
(2) Y.-q. Jiang, S.-h. Jia, X.-y. Li, Y.-m. Sun, W. Li, W.-w. Zhang and G.-q. Xu, *Chemical Papers,* 2018, **72**, 1265-1276.
(3) A.J. Blacker, M. M. Farah, M. I. Hall, S. P. Marsden, O. Saidi and J. M. Williams, *J. Org. Lett.,* 2009, **11**, 2039-2042.
(4) J. Yellol, S. A. Pérez, G. Yellol, J. Zajac, A. Donaire, G. Vigueras, V. Novohradsky, C. Janiak, V. Brabec and J. Ruiz, *Chem. Commun.,* 2016, **52**, 14165 −14168.
(5) B. Erena and Y. Bekdemirb, *Quim. Nova,* 2014, **37**, 643-647.
(6) G. M. Raghavendra, A. B. Ramesha, C. N. Revanna, K. N. Nandeesh, K. Mantelingu and K. S. Rangappa, *Tetrahedron Lett.,* 2011, **52**, 5571–5574.
(7) H. Baars, A. Beyer, S. V. Kohlhepp and C. Bolm, *Org.Lett.,* 2014, **16**, 536−539.

(8) D.-L. Ma, S. Lin, L. Lu, M. Wang, C. Hu, L.-J. Liu, K. Ren and C.-H. Leung, *Mater. Chem. B*, 2015, **3**, 4780-4785.

(9) G.-G. Shan, H.-B. Li, Z.-C. Mua, D.-X. Zhu, Z.-M. Su and Y. Liao, *J. Org. Chem.,* 2012, **702**, 27-35.

(10) J. E. Jones, R. L. Jenkins, R. S. Hicks, A. J. Hallett and S. J. A. Pope, *Dalton Trans.*, **2012**, *41*, 10372.

(11) Zamora, S. A. Pérez, V. Rodríguez, C. Janiak, G. S. Yellol and J. Ruiz, *J. Med. Chem.,* 2015, **58**, 1320-1336.

(12) J. Pracharova, G. Vigueras, V. Novohradsky, N. Cutillas, C. Janiak, H. Kostrhunova, J. Kasparkova, J. Ruiz and V. Brabec, *Chem.-Eur. J.,* 2018, **24**, 4607-4619.

(13) (a) V. Lozan, P.-G. Lassahn, C. Zhang, B. Wu, C. Janiak, G. Rheinwald and H.Z. Lang. *Naturforsch. B*, 2003, **58**, 1152. (b) C. Zhang and C. Janiak, *Z. Anorg. Allg. Chem.*, 2001, **627**, 1972. (c) C. Zhang and C. Janiak, *J. Chem. Crystallogr.,* 2001, **31**, 29. (d) H.-P. Wu, C. Janiak, G. Rheinwald and H. Lang, *J. Chem. Soc. Dalton Trans.,* 1999, 183. (e) C. Janiak, L. Uehlin, H.-P. Wu, P. Klüfers, H. Piotrowski and T.G. Scharmann, *J. Chem. Soc., Dalton Trans.*, 1999, 3121. (f) H.-P. Wu, C. Janiak, L. Uehlin, P. Klüfers and P. Mayer, *Chem. Commun.*, 1998, 2637.

(14) (a) N. J. Farrer, J. A. Woods, L. Salassa, Y. Zhao, K. S. Robinson, G. J. Clarkson, F. S. Mackay and P. J. Sadler, *Angew. Chem. Int. Ed.*, 2010, **49**, 1-5. (b) N. A. Smith, P. Y. Zhang, S. E. Greenough, M. D. Horbury, G. J. Clarkson, D. McFeely, A. Habtemariam, L. Salassa, V. G. Stavros, C. G. Dowson and P. J. Sadler, *Chem. Sci.*, 2017, **8**, 395-404. (c) A. Colombo, M. Fontani, C. Dragonetti, D. Roberto, J. A. G. Williams, R. Scotto di Perrotolo, F. Casagrande, S. Barozzi and S. Polo, *Chem. Eur. J.*, 2019, **25**, 7948-7952. (d) V. Novohradsky, A. Rovira, C. Hally, A. Galindo, G. Vigueras, A. Gandioso, M. Svitelova, R. Bresolí-Obach, H. Kostrhunova, L. Markova, J. Kasparkova, S. Nonell, J. Ruiz, V. Brabec and V. Marchán, *Angew. Chem. Int. Ed.*, 2019, **58**, 6311-6315.

(15) K. W. Dunn, M. M. Kamocka, J. H. McDonald, *Am. J. Physiol. Cell Physiol.* **2011**, *300*, C723-C742.

(16) J. P. Robinson, L. H. Bruner, C. F. Bassoe, J. L. Hudson, P. A. Ward, S. H. Phan, *J. Leukocyte Biol.* **1988**, *43*, 304-310.

(17) (a) S. P.-Y. Li, C. T.-S. Lau, M.-W. Louie, Y.-W. Lam, S. H. Cheng, K. K.-W. Lo, *Biomaterials* **2013**, 34, 7519-7532. (b) M. Ouyang, L. Zeng, K. Qiu, Y. Chen, L. Ji, H. Chao, *Eur. J. Inorg. Chem*. **2017**, 1764-1771. (c) S. Yi, Z. Lu, J. Zhang, J. Wang, Z.-H. Xie, L. Hou, *ACS Appl. Mater. Interfaces,* **2019**. DOI: 10.1021/acsami.9b01205.